Experimental Study of a Single Droplet Impinging Upon a Heated Dry Surface Using Jet Fuel and Biofuel Mixtures

Daniela Ribeiro[1*], Jorge Barata[1], André Silva[1]

[1]University of Beira Interior, AEROG-LAETA, Covilhã, Portugal
*Corresponding author: daniela.santo.ribeiro@ubi.pt

Abstract

The aeronautical sector is dependent on fossil fuels which contribute to a considerable amount of pollutant emissions to the atmosphere. In an attempt to reduce these pollutant emissions in a short period of time and without several changes to the aircraft and their engines, this study focuses on the physical phenomena that happen inside the combustion chamber of an internal combustion engine during fuel injection. However, instead of considering only a conventional jet fuel, an alternative fuel is also investigated. The mixture is composed of at least 50% in volume of conventional jet fuel, as demanded by the current legislation, and a biofuel to decrease the consumption of petroleum-based fuels and to reduce pollutant emissions.

The main goal of this study is to experimentally observe droplet impact on a heated dry stainless-steel surface for different fuel mixtures, impact energies (Weber number between 174 and 955, and Reynolds number between 1099 and 12365), and wall temperatures ($T_w = 20 - 300\ ^\circ C$) to identify the different heat regimes and the physical differences between the distinct sets of impact conditions. To achieve that purpose an experimental setup was designed and built including the acquisition of high-speed images, a droplet dispensing system, a heating device to accurately control the temperature of the target surface and the illumination of the impact site. To enhance the knowledge about the impacts, three different perspectives of the phenomena were captured. The typical front perspective, a second perspective where the camera has a $\approx 20^\circ$ angle to the impact surface to capture more details of the impact, and finally, at a lower frame rate, an isometric perspective to measure the evaporation time. From these data, the impact regimes were identified and the influence of surface temperature, fluid properties, and impact energy was analyzed.

Keywords

Droplet impact, Jet Fuel, Alternative Fuels, Heated Surface

Introduction

Studies about droplet impacts are widely reported in the literature [1] and have diverse applications from spray cooling to fuel injection in internal combustion engines. As known, the civil aviation industry is responsible for a significant portion of atmospheric pollution due to its dependency on fossil fuels. Alternative aviation fuels are required to reduce this problem and fulfill the demand for the decarbonization of the aviation sector by 2050 [2]. With that in mind, in previous studies, single droplet impacts on cold dry and wet surfaces were experimentally tested using jet fuel and biofuel mixtures to simulate the physical processes that take place inside the combustion chamber of an internal combustion engine [3,4]. To continue these studies, wall temperature T_w was added as a new influencing parameter. In this way, the influence of temperature can be assessed, simulating better the conditions inside a combustion chamber.

Droplet impingement upon heated walls is a complex phenomenon. Heat transfer is strongly affected by the relation between the wall temperature T_w and the saturation temperature T_{sat}. The saturation temperature T_{sat} corresponds to the boiling point since it is the temperature at which the liquid boils for a certain saturation pressure Different heat transfer regimes can be observed: film evaporation, nucleate boiling, transition boiling, and film boiling [5]. Film evaporation occurs when the wall temperature is smaller than the saturation temperature $T_w <$

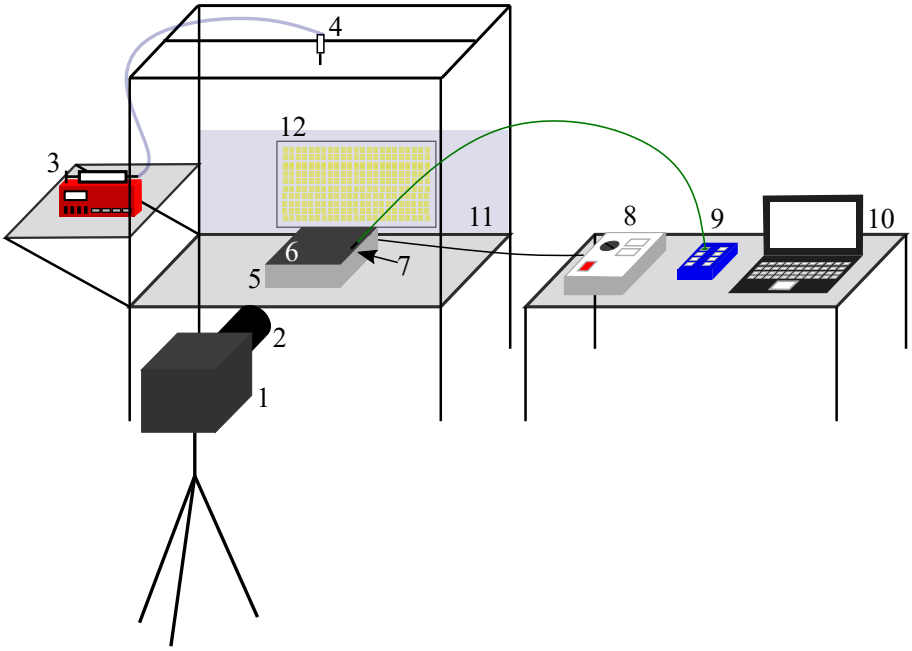

Figure 1. Experimental facility: 1) high-speed digital camera; 2) macro lens; 3) syringe pump; 4) straight tip needle; 5) heating device; 6) stainless-steel impact surface; 7) type-K thermocouple; 8) controller of the heating device; 9) data logger; 10) computer; 11) difussion glass; 12) set of LEDs.

T_{sat}, and nucleate boiling when $T_w = T_{sat}$. On the other hand, transition boiling takes place in the region between the critical heat flux T_{CHF} and the Leidenfrost point T_{Leid}, and film boiling when $T_w > T_{Leid}$. The critical heat flux establishes the shortest droplet lifetime and corresponds to the minimum evaporation time [6]. The Leidenfrost temperature T_{Leid} is the lowest wall temperature of the film boiling regime, firstly observed by J. G. Leidenfrost [7].
Several studies have been made about these heat transfer regimes and the parameters that influence them and their characteristics [5]. In this study, the research question is how the physical properties of biofuels can influence the droplet impact phenomena on heated surfaces in comparison with conventional jet fuel and how different are the heat transfer regimes for similar initial impact conditions? Thus, jet fuel, biofuel, and a mixture of both were experimentally tested on the single droplet impact onto a heated surface with similar impact conditions and the heat transfer regime and their characteristics were analyzed.

Experimental Approach

The experimental study of single droplets impinging on heated surfaces demands an experimental setup with a powerful heating device. A scheme of the experimental facility is present in Fig. 1. It is composed of for main sections: image acquisition system, droplet dispensing unit, the heating system of the impact surface, and the illumination of the impact site.
To visualize the phenomena, a high-speed digital camera Photron FASTCAM mini UX50 and a macro lens Tokina AT-X M100 AF PRO D were used. The camera has a 1.3 Megapixel resolution at frame rates up to 2000 fps (frames per second) and at reduced image resolution for frame rates up to 160000 fps. The lens has a minimum focus distance of 0.3 m, a focal length of 100 mm, a macro ratio of 1:1, and a filter size of 55 mm. To capture the phenomena two different perspectives were captured with the high-speed camera, a lateral perspective and another perspective with a camera inclination of $\approx 20^{\circ}$. A different digital camera with a lower frame rate was also used but only to capture the duration of the droplet lifetime. The droplet dispensing system is composed of a syringe pump NE-1000 connected to a straight-tip needle. At a low pumping rate, of 0.5 ml/min, the droplet was able to leave the needle when gravity exceeds the surface tension forces. The room is kept dark and the only light source in the room is a set of LEDs connected to a power supply. As can be seen in Fig. 1, a diffusion glass was

placed between the light source and the impact location.
The focus of this experimental setup is the heating system of the impact surface. An aluminum block of dimensions 15x15x5 cm has four cartridge heaters of 250 W equally spaced to provide evenly distributed heat to the impact surface. The impact surface is a stainless-steel plate with 0.5 mm of thickness. This plate was placed above the aluminum block and fixed with screw clamps. These clamps were needed since at high surface temperatures T_w the plate edges detach from the aluminum block. This block also has an embedded type-K thermocouple which is connected to the heating device controller. On the controller, it is possible to define the aluminum block temperature in a range from $0 - 500\ ^\circ C$.
Before starting the droplet impact experiments, the heating system was tested. Two type-K thermocouples, connected to the data logger, were placed on the stainless-steel plate, one right in the middle since it is the place where the drop will impinge on, and the other on the side, as represented in Fig. 1. Starting at room temperature, $T_w = 20\ ^\circ C$, the temperature was increased in intervals of $20\ ^\circ C$ in the heating device controller. The surface temperature measured in the center of the place corresponds to the same measured by the type-K thermocouple embedded in the aluminum block. There are no significant thermal losses due to the high conductivity of aluminum and stainless-steel. Regarding the type-K thermocouple placed on the border of the plate, the measured surface temperature is lower than in the center. The maximum temperature deviation is $= 14\ ^\circ C$ for a $T_w = 300\ ^\circ C$ in the center of the plate. These results were saved and the thermocouple on the border of the plate was kept to supervise possible malfunctions in the heating device during the experiments, since the thermocouple in the center has to be removed.

Parameter Space
To study the differences in the heating regimes depending on the thermophysical properties of the fluids, the impact energy, and the surface temperature, a wide range of impact conditions were tested. Four different fluids were used: 100% Jet A-1 (JF), 100% NExBTL (HVO), a mixture with 50% in volume of Jet A-1 and 50% of NExBTL, and distilled water, as a reference. Jet A-1 is a conventional jet fuel widely used in the civil aviation sector and NExBTL is Neste Renewable Diesel, a type of HVO (Hydroprocessed Vegetable Oil). Civil aviation only allows fuel blends with at least 50% in volume of a conventional jet fuel [8,9] and that is why the blend with 50% of each type of fuel was chosen. The fluid properties, density, surface tension, and viscosity at $20\ ^\circ C$ are presented in Table 1, as well, as the final boiling point. These properties were given by previous studies and by the fuel suppliers [3,10]. For the 50%/50% fuel blend, the final boiling point value is not available.

Table 1. Fluid Properties: density ρ, surface tension σ, viscosity μ and final boiling point [3,10].

	Jet A-1	50%JF-50%HVO	NExBTL	H_2O
$\rho\ [kg/m^3]$	798.3	792.3	785.2	1000
$\sigma \cdot 10^3\ [N/m]$	25.4	24.6	26.6	72.0
$\mu \cdot 10^3\ [Pa \cdot s]$	1.12	1.79	3.40	1.00
Final Boiling Point ($^\circ C$)	237	-	300	100

Using these fluids, the parameter space is described in Table 2. The surface temperature T_w varied between $20 - 300\ ^\circ C$. The inner diameter of the needle was kept constant at $D_{in} = 1.2\ mm$ giving droplet initial diameters D_0 between $2.8 - 3.8\ mm$. The impact velocity U_0 was varied by changing the impact height. Using two different impact heights, U_0 varied between 1.7 and $3.2\ mm$. Weber We and Reynolds numbers Re were as important influencing parameters. The Weber number describes the ratio between the inertial and surface tension forces, $We = \rho D_0 U_0^2/\sigma$, and the Reynolds number is the ratio between the inertial and viscous forces, $Re = \rho D_0 U_0/\mu$. In this study, the values ranged between $174 < We < 955$ and $1099 < Re < 12365$.

Table 2. Summary of the parameters used in this study: wall temperature T_w, droplet initial diameter D_0, impact velocity U_0, Weber number We, and Reynolds number Re.

$T_w\ [^\circ C]$	$D_0\ [mm]$	$U_0\ [m/s]$	We	Re
20-300	2.8-3.8	1.7-3.2	174-955	1099-12365

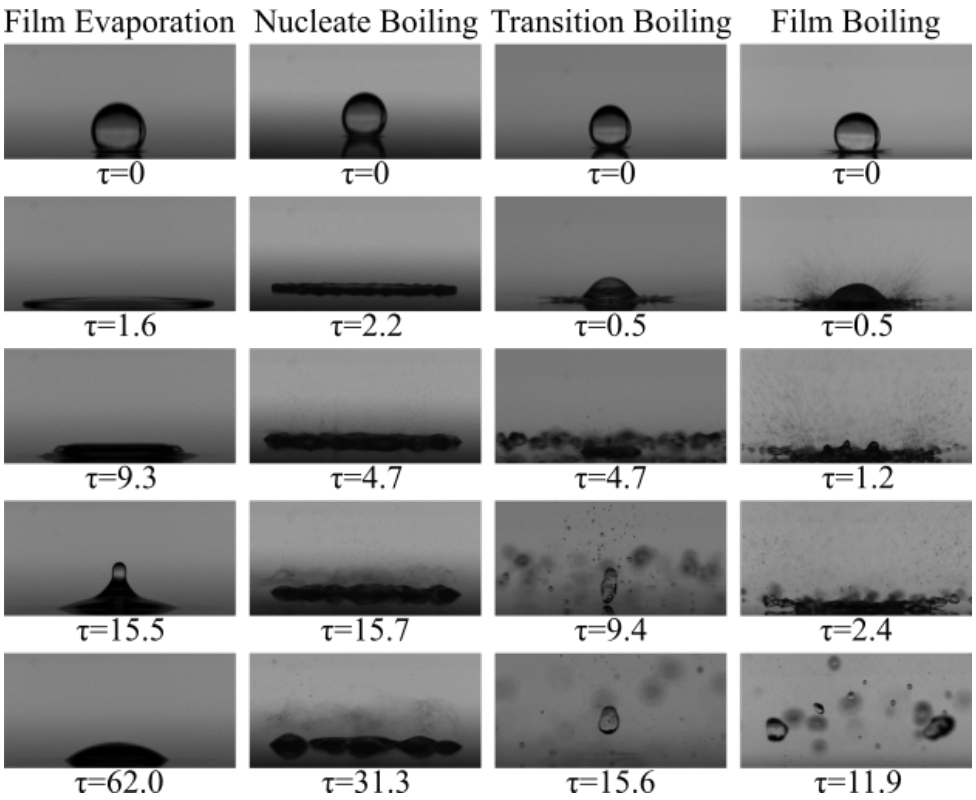

Figure 2. Heat Transfer Regimes: Film evaporation for 100% NExBTL at We=244 and Re=1099 at $T_w = 220\ ^\circ C$, Nucleate Boiling for 50% Jet A-1 - 50% NExBTL for We=305 and Re=2311 at $T_w = 300\ ^\circ C$, Transition Boiling for 100% Jet A-1 for We=299 and Re=3746 at $T_w = 300\ ^\circ C$, and Film Boiling for distilled water for We=174 and Re=6930 at $T_w = 300\ ^\circ C$.

Results and Discussion

In the following sections, the results will be presented and discussed. First, a description of the heat transfer regimes depending on the Weber number, Reynolds number, and surface temperature. Then, some considerations about the hydrodynamic impact regimes and their differences between fluids. Finally, the evaporation time measurements will be presented and discussed.

Heat Transfer Regimes

Within the parameter space, all four heat transfer regimes were observed: film evaporation, nucleate boiling, transition boiling. and film boiling. Figure 2 shows an image sequence example of each heat transfer regime. Every frame is identified with its dimensionless time $\tau = tU_0/D_0$, where t is time after impact. Film evaporation usually occurs when $T_w < T_{sat}$. The film evaporation sequence in Fig. 2 corresponds to the droplet impact of 100% NExBTL with $We = 244$ and $Re = 1099$ at $T_w = 220\ ^\circ C$. This is the fluid with the highest final boiling point (Tab. 1). As can be seen, the droplet spreads on the surface and, in this case, it quickly recedes and forms a small jet. Then, it stays on the surface and becomes thinner due to evaporation.

Increasing T_w, the nucleate boiling regime begins. This regime is characterized by $T_w = T_{sat}$. In Fig. 2, a 50% Jet A-1 - 50% NExBTL droplet with $We = 305$ and $Re = 2311$ impinges the surface with $T_w = 300\ ^\circ C$. The droplet spreads on the surface, breaks into puddles, and starts to boil. This regime is well known for the formation of pagoda-like bubbles, which also occur in these experiments.

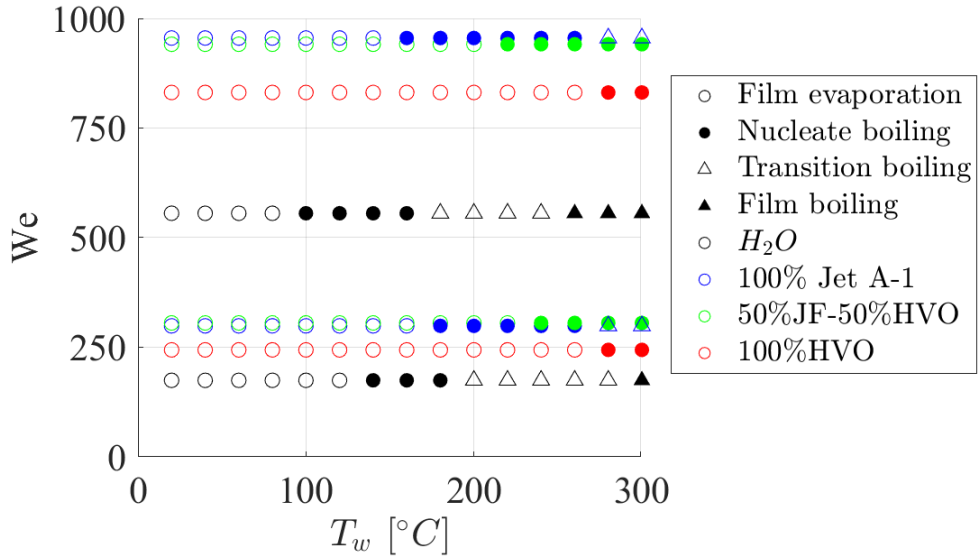

Figure 3. Heat transfer regimes map depending on the wall temperature T_w and on the Weber number We for all fluids. The heat transfer regimes are identified by the different symbols, empty and filled, and the fluids are identified by different colors. Black for distilled water, blue for 100% Jet A-1, green for 50%JF-50%HVO, and red for 100% NExBTL.

The third sequence in Fig. 2 represents the transition boiling regime, where $T_{CHF} < T_w < T_{Leid}$. In this regime, the contact between the droplet and the surface is intermittent. The droplet is able to "levitate" due to the tiny unstable vapor layer beneath it. The sequence shows a 100% Jet A-1 droplet impinging on the stainless-steel surface at $T_w = 300\ ^\circ C$, $We = 299$, and $Re = 3746$. After impact, secondary atomization is produced and after droplet shattering a large droplet remains "levitating" on the surface in the so-called drop dancing phenomenon.
Finally, the film boiling regime, $T_w > T_{Leid}$, for a distilled water droplet impact with $We = 174$, $Re = 6930$, and $T_w = 300\ ^\circ C$. In this regime, there is no contact between the liquid and the solid. After impact, the droplet shatters completely.
One of the goals of this study is to observe the differences in the heat transfer regimes depending on the fluids. Figure 3 shows a heat transfer regime map depending on the wall temperature T_w and on the Weber number We for all fluids. The different fluids are identified by different colors: black for distilled water, blue for 100% Jet A-1, green for 50%JF-50%HVO, and red for 100% NExBTL. The heat transfer regimes are identified by different symbols. Looking at Fig. 3, it is noticeable that 100% NExBTL originated the same heat transfer regimes independently of the impact energy. For the other three fluids, at higher impact energies the transition for the following heat transfer regime happens for lower wall temperatures than at lower impact energies. Distilled water is the only fluid that reached the film boiling regime for the range of wall temperatures tested, which is justified by its low boiling point. Despite having similar Weber number values to the 50%/50% mixture, the 100% Jet A-1 reaches nucleate boiling and transition boiling at significantly lower wall temperatures.
Additionally, to evaluate the influence of the Reynolds number in the heat transfer regimes, Fig. 4 shows a heat transfer regime map depending on the wall temperature T_w and on the Reynolds number Re for all fluids. The same symbols and colors scheme was kept. From this plot, it is easier to understand the differences between the fluids regarding reaching the same heat transfer regime at different wall temperatures. Due to its high viscosity, 100% NExBTL shows the lowest Reynolds number values and it is also the fluid with the higher final boiling point. In this way, it only transitions to nucleate boiling at $T_w = 280\ ^\circ C$. In general, increasing the Reynolds number will help to reach the same heat transfer regime at lower wall temperatures.

Evaporation Time

As explained before, a third perspective of the phenomena was captured by a digital camera at a lower frame rate. This perspective has the purpose of capturing the droplet evaporation

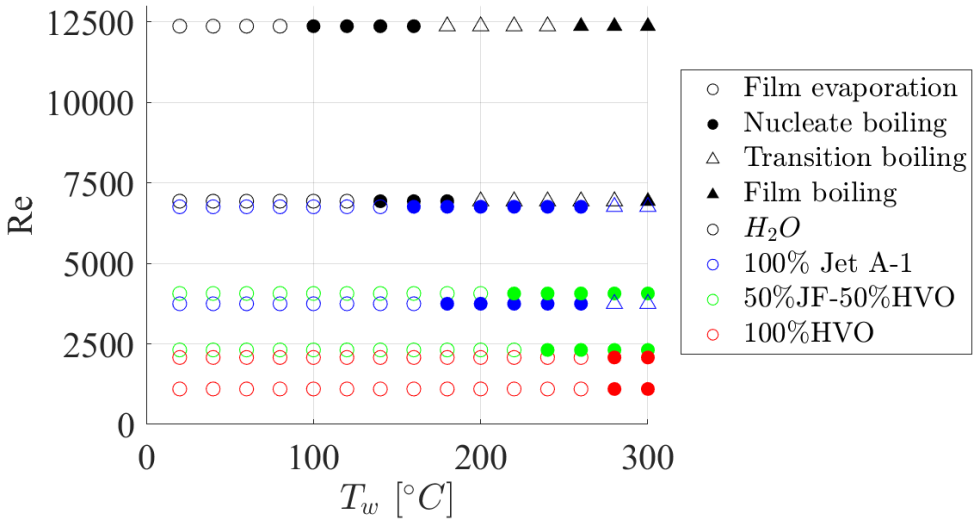

Figure 4. Heat transfer regimes map depending on the wall temperature T_w and on the Reynolds number Re for all fluids. The heat transfer regimes are identified by the different symbols, empty and filled, and the fluids are identified by different colors. Black for distilled water, blue for 100% Jet A-1, green for 50%JF-50%HVO, and red for 100% NExBTL.

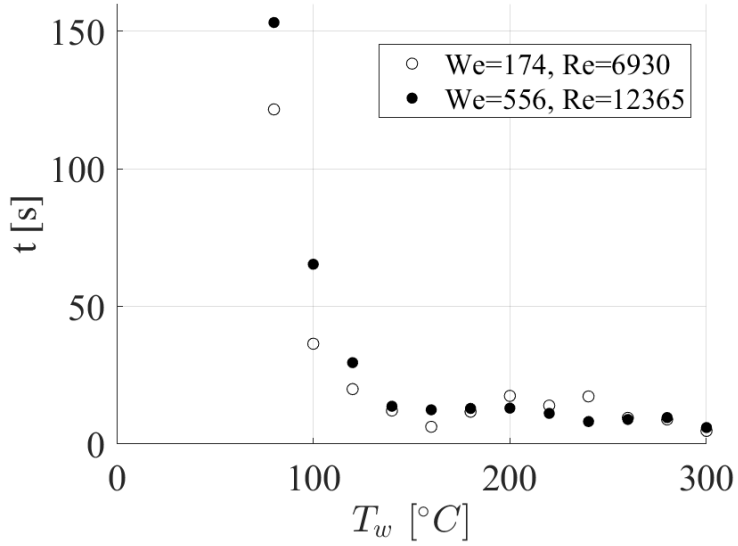

Figure 5. Evaporation time for a distilled water droplet depending on wall temperature for two different impact energies.

time. Using these images, the impact frame and the last frame where there is still a part of the droplet on the stainless-steel plate were identified.

Figure 5 shows the evaporation time for a distilled water droplet for the two impact energies studied. The horizontal axis is the wall temperature T_w and the vertical axis is the time after impact t. The evaporation time was measured for $T_w \geq 80\ ^\circ C$. For the lower impact energy $We = 174$, at $T_w = 80\ ^\circ C$ the evaporation time is $\approx 120\ s$. Increasing the wall temperature the evaporation time drastically decreases until $T_w = 140\ ^\circ C$, within the nucleate boiling regime. Then, slightly oscillates until reaching the lowest evaporation time for $T_w = 300\ ^\circ C$.

For the higher impact energy $We = 556$, at $T_w = 80\ ^\circ C$ the evaporation time is higher $\approx 150\ s$. Increasing the wall temperature the evaporation time also drastically decreases until $T_w = 160\ ^\circ C$, which marks the boundary between the nucleate boiling and transition boiling regimes. After that, the evaporation time also slightly oscillates until reaching the lowest evaporation time for $T_w = 300\ ^\circ C$.

The evaporation time is also measured for the fuels but even after 30 minutes there still remains fluid on the stainless-steel surface. All fuels used are multi-component substances and that could be the reason for the delayed evaporation.

Conclusions

In this study, a single droplet impact onto a dry heated surface was experimentally investigated. With the purpose of reducing the fuel consumption of the aviation sector and also the pollutant emissions, jet fuel and biofuel were the working fluids. For the experimental conditions used, all four heat transfer regimes were observed: film evaporation, nucleate boiling, transition boiling, and film boiling.

Considering the differences in the heat transfer regimes depending on the fluids, 100% NExBTL shows the same heat transfer regimes independently of the impact energy, and since it presents the higher boiling point only transitions to the nucleate boiling regime at $T_w = 280\ ^\circ C$. For the other fluids, an increase in the impact energy decreases the wall temperature needed to reach the following heat transfer regime. Only distilled water reached the film boiling regime which is justified by its low boiling point. Despite the similarities between 100% Jet A-1 and the 50%/50% mixture, jet fuel is able to reach the nucleate boiling and transition boiling at significantly lower wall temperatures. Finally, the evaporation time for a distilled water droplet is presented.

Acknowledgements

The present work was performed under the scope of Laboratório Associado em Energia, Transportes e Aeronáutica (LAETA) activities, and it was supported by Fundação para a Ciência e a Tecnologia (FCT) through the project UIDB/50022/2020, and also the Ph.D. grant SFRH/BD/140009/2018.

Nomenclature

D_0	initial droplet diameter [m]
D_{in}	needle inner diameter [m]
Re	Reynolds number [-]
t	time after impact [s]
T_{CHF}	critical heat flux temperature [$^\circ C$]
T_{Leid}	Leidenfrost temperature [$^\circ C$]
T_{sat}	saturation temperature [$^\circ C$]
T_w	wall temperature [$^\circ C$]
U_0	impact velocity [m/s]
We	Weber number [-]
μ	viscosity [Pa·s]
ρ	density [kg/m^3]
σ	surface Tension [N/m]
τ	dimensionless time [-]

References

[1] Yarin, A.L., Roisman, I.V. and Tropea, C., 2017,'Collision phenomena in liquids and solids'. Cambridge University Press.
[2] Abrantes, I., Ferreira, A.F., Silva, A. and Costa, M., 2021, *Journal of Cleaner Production*, 313, p.127937.
[3] Ribeiro, D.F., Silva, A.R. and Panão, M.R., 2020, *Applied Sciences*, 10(19), p.6698.
[4] Ferrão, I., Vasconcelos, D., Ribeiro, D., Silva, A. and Barata, J., 2020, *Fuel*, 279, p.118321.
[5] Liang, G. and Mudawar, I., 2017, *International Journal of Heat and Mass Transfer*, 106, pp.103-126.
[6] Katto, Y., 1994, *International Journal of Multiphase Flow*, 20, pp.53-90.
[7] Leidenfrost, J.G., 1966, *International Journal of Heat and Mass Transfer*, 9(11), pp.1153-1166.
[8] ASTM D1655-19a, Standard Specification for Aviation Turbine Fuels, 2019, Technical Report, USA.

[9] ASTM D7566-19b, Standard Specification for Aviation Turbine Fuel Containing Synthesized Hydrocarbons, 2019, Technical Report, USA.
[10] Pacheco, G., Silva, A. and Costa, M., 2021, *Energy Fuels*, 35(9), pp.7232-7241.